ACS Energy LETTERS

Open Access

http://pubs.acs.org/journal/aelccp

Letter

Compositional Analysis of Metal Halide Perovskites: Insight into the Coevaporation Process via Nuclear Magnetic Resonance and X-ray Fluorescence Spectroscopy

Marcel Roß,* Stefanie Severin, Jana Hildebrandt, Kerstin Erdmann, Aleksandra Miaskiewicz, Viktor Škorjanc, Wander Max Bernardes de Araujo, Matthew Leyden, Lars Korte, Stefan Seeger, André Dallmann, and Steve Albrecht

Cite This: *ACS Energy Lett.* 2026, 11, 1935−1943

Read Online

ACCESS | Metrics & More | Article Recommendations | Supporting Information

ABSTRACT: Lead halide perovskites have emerged as a highly promising class of materials for solar cells. Nevertheless, suitable procedures to analyze the exact composition of the perovskite films are rare and are not generally applicable. Here we show a simple and fast method to determine the absolute composition of mixed metal halide perovskites through a combination of nuclear magnetic resonance and total reflection X-ray fluorescence spectroscopy. The method is validated on powder mixtures and applied to thin film samples prepared by coevaporation of formamidinium iodide (FAI), CsI, PbI_2 and $PbBr_2$, allowing correlation between film composition and solar cell performance. We show that the rates of the individual precursors do not always translate linearly into film composition and that the preparation of the hole transport layer MeO-2PACz strongly influences the incorporation of FAI. Our work highlights the importance of compositional analysis and demonstrates how the developed method provides new insights into the complex coevaporation process in perovskite solar cells.

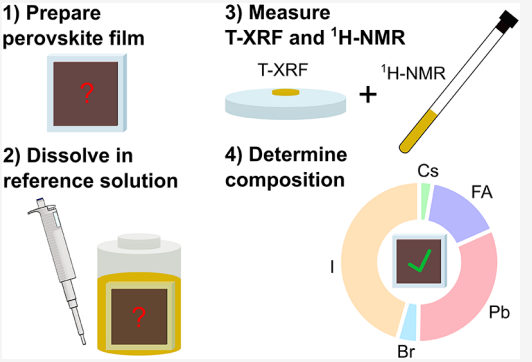

Metal halide perovskite solar cells have gained significant attention over the past decade due to their low-cost fabrication methods and high efficiency potential. Typically, perovskite films are prepared by solution-based deposition techniques, which allow for rapid deposition and a wide variety of compositions.[1] However, achieving conformal coverage on textured surfaces, which is particularly important for industry-relevant monolithically integrated perovskite/silicon tandem solar cells, can be challenging with these techniques. Additionally, creating compositional gradients, for example, to form graded Fermi Levels in the absorber material, is also complicated when using solution-based depositions. These limitations can be overcome by coevaporating the perovskite precursor materials.[2−5]

To form perovskite absorbers with band gaps of 1.65 to 1.70 eV, well suited for perovskite/silicon tandem solar cells, typically mixtures of formamidinium, cesium, lead, bromide and iodide precursors are used in vapor deposition processes.[6−8]

In contrast to solution-based deposition processes where the stoichiometry is dictated by the concentration of the individual precursors in the solution, the composition in coevaporation processes is typically governed by the evaporation rates of the precursors, conventionally measured using quartz crystal microbalances (QCMs).[9] However, accurately determining the composition from these rates is challenging as the formation of the perovskite involves complex chemical reactions, which highly depend on a variety of parameters. For example, it was shown that substrate temperature,[10,11] surface properties of the underlying charge selective contact,[12,13] pressure in the evaporation chamber as well as purity of the precursor materials can change the composition of the perovskite prepared with nominally identical evaporation rates.[14−16] The larger the number of materials simultaneously evaporated, the more complex the estimation of the composition is based on the evaporation rates. Therefore, the subsequent analysis of the perovskite composition is of decisive importance.

However, analyzing the composition of perovskite films is rather challenging due to the limited amount of material resulting from the low layer thickness of typically 500−600 nm. In addition, the mixture of light elements such as (C, H, N) and heavy elements such as (Pb, I) complicates the analysis with a single method.[17] Scanning electron microscopy, coupled

Received: November 7, 2025
Revised: December 18, 2025
Accepted: December 19, 2025
Published: January 12, 2026

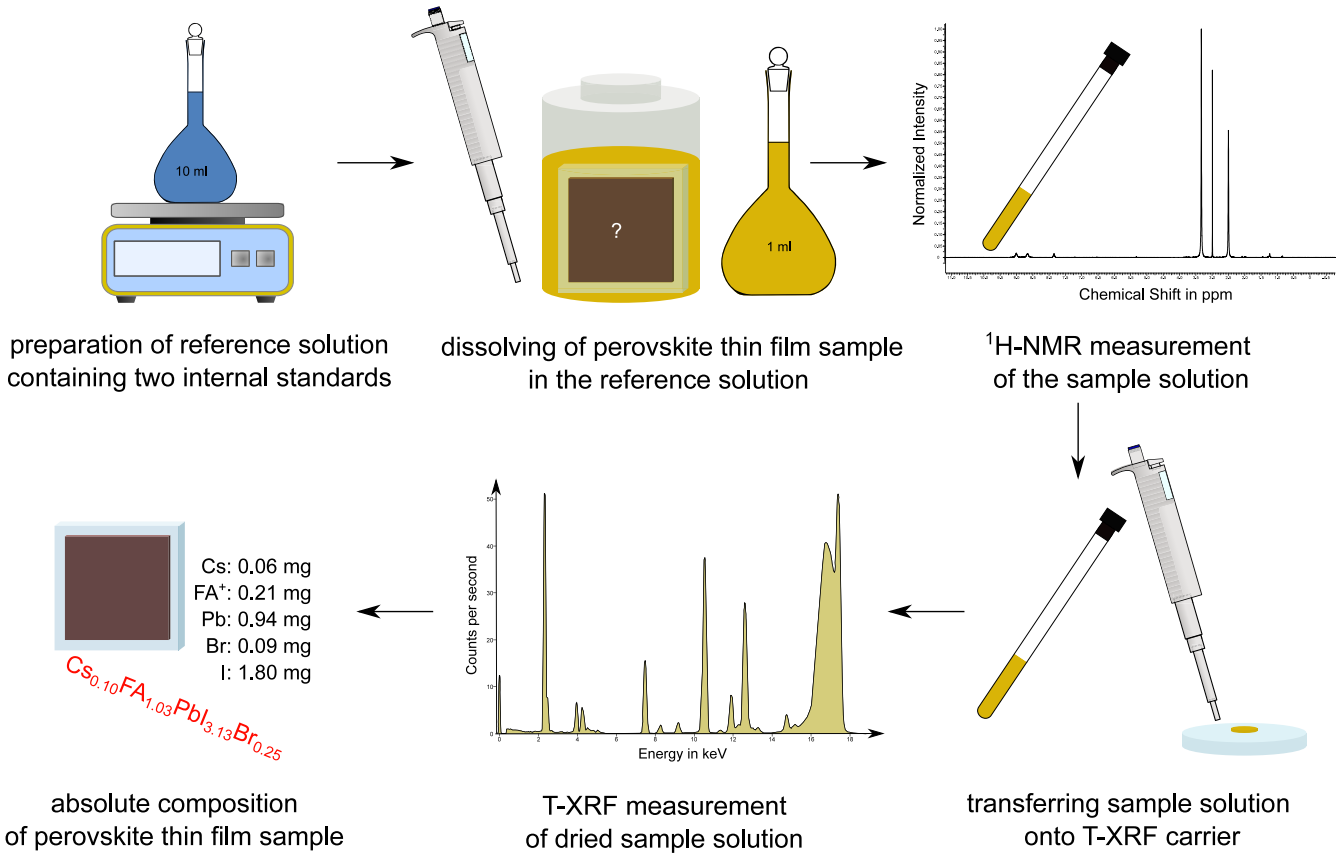

Figure 1. Schematic illustration of the developed procedure to determine the absolute composition of mixed metal halide perovskites. The perovskite film on the sample is dissolved in a reference solution, containing two internal standards, $DMSO_2$ for the ^1H NMR analysis and $Ni(NO_3)_2{\cdot}6H_2O$ for the T-XRF measurements.

with energy-dispersive X-ray spectroscopy (SEM-EDX), X-ray fluorescence (XRF), and inductively coupled plasma mass spectrometry (ICP-MS) have been reported to determine the heavy elements, especially the lead to iodine ratio, of different perovskites.[18−21] These methods are not well suited for determining very light elements,[22−24] and even for the inorganic components of the perovskite, each method has its specific set of challenges. For example, in ICP-MS measurements the quantification of halides is not trivial,[25,26] as the frequently used elemental standards typically contain nitric acid and can cause oxidation reactions and thus a change in composition.[27−29]

In XRF, the typical excitation depth is, depending on density of the material, in the range of 1 to 2 μm. Due to the typical perovskite film thickness of 500−600 nm in PV applications, this can lead to strong background signals from the substrate and therefore to rather high detection limits.[30] For total reflection X-ray fluorescence spectroscopy (T-XRF) an incidence angle below the total reflection angle is used.[31] This reduces the level of penetration of the primary radiation into the substrate and consequently improves the signal-to-noise ratio. In contrast to conventional XRF, the quantity of an element in thin samples is directly proportional to the respective fluorescence signal.[32] Therefore, for T-XRF the absolute quantification can be easily done using internal calibration standards.[30,32]

In order to analyze the organic part of the perovskite, hydrogen nuclear magnetic resonance spectroscopy (^1H NMR) can be used.[5,17] Pareja-Rivera et al. demonstrated a method in which the perovskite material is scraped off the substrate, and the obtained powder is scaled. Afterward, the perovskite powder was dissolved in an internal standard solution (1,2,4,5-tetrachloro-3-nitrobenzene in DMSO). From the absolute mass of the sample in combination with the amount of organic precursors (FAI and MAI) quantified by NMR, the total amount of cesium was calculated. The method requires perovskite in a phase-pure stochiometric ($Cs_xFA_yMA_zPbI_3$ with $x + y + z = 1$) form, free of inhomogeneities and impurities, as only the total mass and the amount of FA and MA are directly measured. Another limitation of the method is the large amount of sample material required for accurate weighing. Approximately 15 mg of perovskite powder is necessary, which corresponds to about 15 films with an area of 6 cm^2.[17]

X-ray photoelectron spectroscopy (XPS) allows for the determination of both the organic (C, N) and inorganic components of the perovskite. XPS is an established method for measuring the composition of perovskites.[13,33,34] Unfortunately, the measurement takes place in a high vacuum under X-ray irradiation, which can lead to degradation of the material and can cause changes in the perovskite composition.[35−37] Furthermore, XPS is highly surface-sensitive, probing only a few nanometers of the top and thus making the quantification of the composition for bulk materials very difficult.

All in all, despite various applied techniques, the compositional analysis of metal halide perovskites is not trivial, and well-established methods are missing. Here we present a simple and fast procedure to determine the absolute

https://doi.org/10.1021/acsenergylett.5c03689
ACS Energy Lett. 2026, 11, 1935−1943

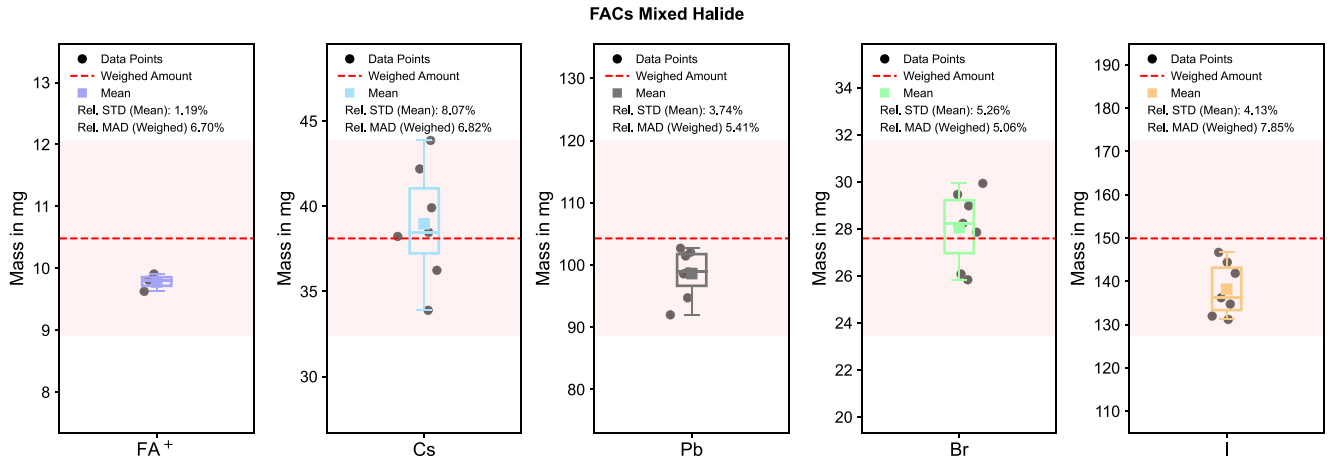

Figure 2. Analysis of the FACs Mixed Halide test sample containing a mixture of 40.1 mg of FAI, 74.5 mg of CsI, 152.4 mg of PbI_2, and 63.4 mg of $PbBr_2$. Dashed red lines indicate the scaled amount and the light red shaded areas represent a ±15% tolerance range around it. Individual data points for repeated measurement of the test sample solution are shown as black dots, and colored squares mark the arithmetic mean value. Relative standard deviation (Rel. STD (Mean)) based on the arithmetic mean and relative median absolute deviation (Rel. MAD (Scaled)) based on the scaled amount are displayed in the legend.

composition of mixed metal halide perovskite thin films and powders. By using a combination of nuclear magnetic resonance spectroscopy (NMR) and total reflection X-ray fluorescence spectroscopy (T-XRF), we can quantify all components of the perovskite material. Using a standard solution consisting of two internal standards simplifies the sampling process, allowing for the use of the same solution in both measurements. With the developed method we analyze perovskite samples prepared by coevaporation of formamidinium iodide (FAI), CsI, PbI_2 and $PbBr_2$. We show how the evaporation rates and the preparation of the underlying hole transporting material [2-(3,6-dimethoxy-9*H*-carbazol-9-yl)-ethyl]phosphonic acid (MeO-2PACz)[38] are influencing the composition of the films. We correlate the results with structural and optoelectronic properties of the resulting p-i-n solar cells and show the importance of compositional analysis for optimizing the coevaporation process.

A major problem with some of the existing methods for absolute compositional quantification is that the perovskite material must be scratched from the substrate and carefully scaled to determine the absolute composition.[17] In order to simplify the sampling process, we developed a method in which the perovskite film is dissolved and removed from the substrate. Figure 1 shows a schematic of this method. First, two commercially available chemicals, dimethyl sulfone ($DMSO_2$) and nickel(II) nitrate hexahydrate ($Ni(NO_3)_2{\cdot}6H_2O$), are scaled and dissolved in a known amount of dimethyl sulfoxide (DMSO) to obtain a reference solution. Here the $DMSO_2$ is used as a standard for the ^{1}H NMR spectroscopy, and the nickel acts as standard for the T-XRF measurements. In principle, other chemicals can also be used for the reference solution, but it is important to ensure that no oxidizing standards are used. Otherwise, the halides such as bromide and iodide will be oxidized, resulting in a visible change in color due to the formation of highly volatile bromine and iodine (Figure S1). This restriction means that classic ICP-MS and T-XRF standards, which often contain nitric acid,[29] are unsuitable for the analysis. To transfer all of the perovskite material into solution, the sample is extracted several times with a defined amount of the reference solution. Here the entire sample can be dissolved, and no scraping or scaling of the perovskite is needed. The sample solution is afterward analyzed by ^{1}H NMR spectroscopy and the signals of the methine group (CH) of FAI and the methyl (CH_3) groups of the $DMSO_2$ are integrated. As the integrated peak area of each signal is directly proportional to the number of protons, the amount of FA^+ in the solution can be determined using the known amount of CH_3 in the standard.

Due to differences in the chemical environment, two separate proton signals can be seen for FAI in the ^{1}H NMR spectrum. In principle, both signals, the CH functions (~3 ppm) and the signals of the NH_2/NH_2^+ groups (~8.7 ppm), can be used for quantification, but due to exchange processes that result in peak broadening of the NH_2/NH_2^+ signals, the use of the CH signal is preferred. As the sample solution remains unchanged during the ^{1}H NMR measurement, it can be directly used to determine the amount of the inorganic components by T-XRF spectroscopy. For this purpose, a defined quantity of the sample solution is deposited on a sample carrier. As soon as the drying process is complete, the T-XRF analysis is carried out using an excitation energy of ~17,5 keV (molybdenum). Due to the known amount of nickel on the sample carrier, originating from the standard solution, the masses of Cs, Pb, I, and Br can be determined. With this simple method, both the organic cations and the inorganic components of the metal halide perovskites can thus be absolutely quantified. More details of the compositional analysis procedure, including the calculation, are shown in the experimental section of the Supporting Information.

To determine the accuracy and spread of the developed method, we analyzed different test samples containing known amounts of perovskite precursors. Therefore, four different combinations of up to five precursor powders were carefully scaled and afterward dissolved in reference solutions. It is important to note that we did not use certified reference chemicals but common lab chemicals, which may deviate from the nominal composition. For lead iodide for example it was shown that the Pb to I ratio can range between $PbI_{1.84}$ and $PbI_{2.1}$.[39] Consequently, the test sample composition is also prone to errors as only standard chemicals were manually weighed. Figure 2 displays the results of the analysis for the mixture of FAI, CsI, PbI_2, and $PbBr_2$ which we denoted as

https://doi.org/10.1021/acsenergylett.5c03689
ACS Energy Lett. 2026, 11, 1935−1943

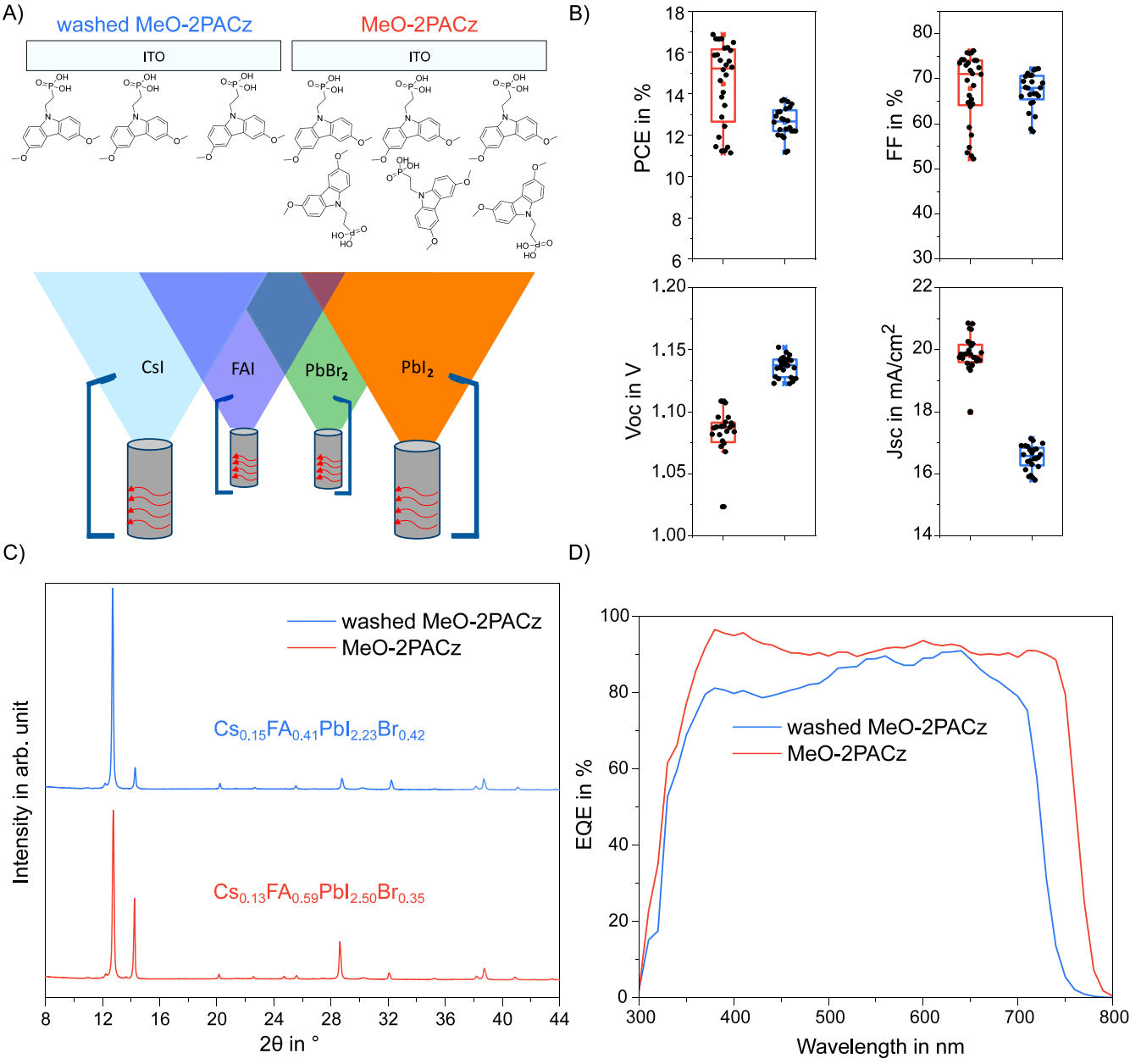

Figure 3. (A) Schematic illustration of the coevaporation process. ITO substrates covered with MeO-2PACz after deposition and after an additional solvent treatment ("washing") step as HTL are used. (B) Characteristic performance parameters of at least 10 different solar cells per group prepared on glass/ITO/MeO-2PACz (red) and washed MeO-2PACz (blue) substrates. The boxes are determined by the 25th and 75th percentiles, the squares represent the mean values, and the horizontal lines represent the median. (C) XRD patterns of perovskite films prepared on MeO-2PACz (red) and washed MeO-2PACz (blue). The displayed relative composition was determined by using the combination of ^{1}H NMR and T-XRF. Therefore, the absolute values were normalized to the amount of lead. (D) Corresponding EQE spectra of solar cells prepared on the two differently prepared HTLs.

FACs Mixed Halide. The content of FA^+ was determined by ^{1}H NMR spectroscopy, while all other elements were quantified by T-XRF measurements. For all components of the test sample, the measured values are in good agreement with the content expected from scaling the powders. For FA^+ the spread between the single measurements is represented by the relative standard deviation (Rel. STD (Mean)) is, with 1.2%, very low, which confirms the high reproducibility of the ^{1}H NMR measurements. Also, the deviation from the scaled amount, represented by the relative median absolute deviation (Rel. MAD (scaled)), is with 6.7%, which is reasonable, especially when considering that no certified reference materials were used to prepare the test samples. Rel. STD (Mean) and Rel. MAD (scaled) values are also below 10% for all other components, which indicates a high accuracy of the method. Compared with the values of Pb and Br, the measurements of Cs and I have a slightly higher Rel. STD (mean). This might be attributed to a small superposition of the I and Cs signals in the T-XRF spectrum, as the emission energy of Cs ($L\alpha_1 \sim 4.29$ keV) and I ($L\alpha_1 \sim 3.94$ keV) are in the same range. In addition to the FACs Mixed Halide sample, we also analyzed FAI + MABr, PbI_2 + CsBr and Triple-cation test samples. These results are shown in Figures S2–S4. For all tested samples, the Rel. STD (mean) and Rel. MAD (scaled)

https://doi.org/10.1021/acsenergylett.5c03689
ACS Energy Lett. 2026, 11, 1935−1943

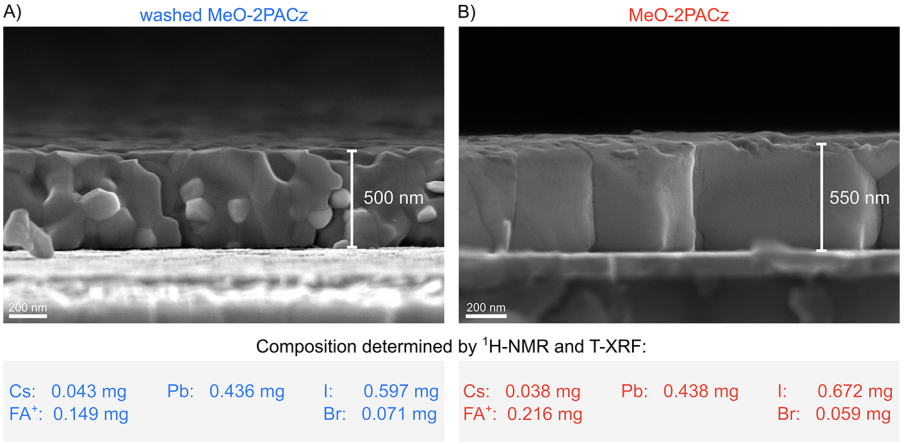

Figure 4. Cross-sectional SEM images of perovskite films prepared by coevaporation on (A) washed MeO-2PACz and (B) MeO-2PACz. The absolute mass for the 2.5 × 2.5 cm^2 samples was quantified by the newly developed method using NMR and T-XRF.

values are smaller than 10%, indicating a high accuracy independent of the perovskite precursor mixture.

In the next step, we use the developed method to determine the composition of perovskites prepared by coevaporation of PbI_2, $PbBr_2$, CsI and FAI. In Figure 3A a schematic of the coevaporation process is shown. As substrates, we use indium tin oxide coated glass covered with MeO-2PACz as a hole transporting layer (HTL). If the MeO-2PACz layer is first deposited via spin coating and afterward washed with its former solvent (ethanol), unbound molecules are removed, and a proper self-assembled monolayer is formed. If washing after spin coating is omitted, then unbound molecules with free phosphonic acid groups remain. Both the washed case and the pristine MeO-2PACz case are displayed schematically in Figure 3A. Further details of the two different ways to prepare the MeO-2PACz layer are described in the experimental section in the Supporting Information. Figure 3B shows how the preparation of MeO-2PACz influences the corresponding solar cell performance. All solar cells have been prepared in the same coevaporation process and use the same solar cell layout with an active area of 0.16 cm^2. On pristine MeO-2PACz a maximum power conversion efficiency (PCE) of 16.8% is reached, while the highest PCE on washed MeO-2PACz is limited to 13.7%. However, the spread of the solar cell PCE values is significantly lower on washed MeO-2PACz. The most significant differences can be observed in open circuit voltage (V_{OC}) and short-circuit current density (J_{SC}). The cells on pristine MeO-2PACz have a V_{oc} of approximately 1.09 V, while the cells on washed MeO-2PACz reach a V_{oc} of about 1.14 V. The solar cells prepared on pristine MeO-2PACz have a considerably higher J_{sc}. For pure $FAPbI_3$, it has already been shown that the deposition method of MeO-2PACz can influence the performance of coevaporated perovskite solar cells. This is attributed to a different growth process and an associated change in perovskite composition.[40,5] In particular, it was observed that the FAI rate during the coevaporation process must be reduced by approximately 30% to achieve similar solar cell efficiencies on pristine MeO-2PACz compared to washed MeO-2PACz.[40]

With the combination of NMR and T-XRF, we measured the composition of the perovskites used in solar cells. The Cs content of the samples normalized to lead is with 0.13 and 0.15 mol rather comparable. In contrast, the FA^+ fraction of the perovskite normalized to lead is considerably different with 0.41 mol on washed MeO-2PACz and 0.59 mol on pristine MeO-2PACz. This difference in FA^+ content agrees well with the change in FAI incorporation for pure $FAPbI_3$ observed in the literature.[40] Figure 3C shows XRD patterns of films prepared on MeO-2PACz (red) and washed MeO-2PACz (blue). Both films contain an excess of PbI_2, which can be seen from XRD and as well from the $(Cs+FA^+)/Pb$ ratio below 1. In comparison to pristine MeO-2PACz, the XRD pattern on washed MeO-2PACz shows a significantly higher intensity ratio of lead iodide (peak at 12.6°) to perovskite (peak at 14.0°), which fits well to the measured composition. Overall, XRD and composition analysis prove that the altered incorporation of FAI observed for pure $FAPbI_3$ also applies to the more complex coevaporation of PbI_2, $PbBr_2$, CsI and FAI. Interestingly, the observed differences in FAI incorporation directly influence the Br/I ratio. The Br/I ratio on MeO-2PACz (0.14) is smaller than that of the washed MeO-2PACz (0.18). This is a consequence of the lower incorporation of FAI into washed MeO-2PACz. The different Br/I ratios are directly reflected in the band gap of the perovskite. Figure 3D displays the EQE spectra and illustrates a band gap difference of 0.08 eV between PSCs prepared on washed and pristine MeO-2PACz. The strong impact of the MeO-2PACz preparation on the perovskite growth has so far only been observed for coevaporated perovskites. Figure S5 shows a comparison of pristine MeO-2PACz and washed MeO-2PACz for perovskites prepared by spin-coating. The composition analysis showed no significant differences between pristine and washed MeO-2PACz. In comparison to coevaporated perovskites, the band gap and solar cell performance parameters are very similar on washed MeO-2PACz and pristine MeO-2PACz. A possible reason for this is that in spin-coated perovskite films, the unbound MeO-2PACz molecules are dissolved by the DMF/DMSO in the perovskite precursor solution and do not strongly influence the interface and the growth of the perovskite. In contrast, the growth of the perovskite during coevaporation has been proven to be very sensitive on the substrate and transporting layer.[2,11−13,40−43]

A particular advantage of the developed method is that the absolute composition of the perovskite is directly accessible. Figure 4 shows cross-sectional SEM images of perovskite films on MeO-2PACz (red) and washed MeO-2PACz (blue). The text below the image reports the mass of each material component obtained from a 2.5 × 2.5 cm^2 large perovskite

https://doi.org/10.1021/acsenergylett.5c03689
ACS Energy Lett. 2026, 11, 1935−1943

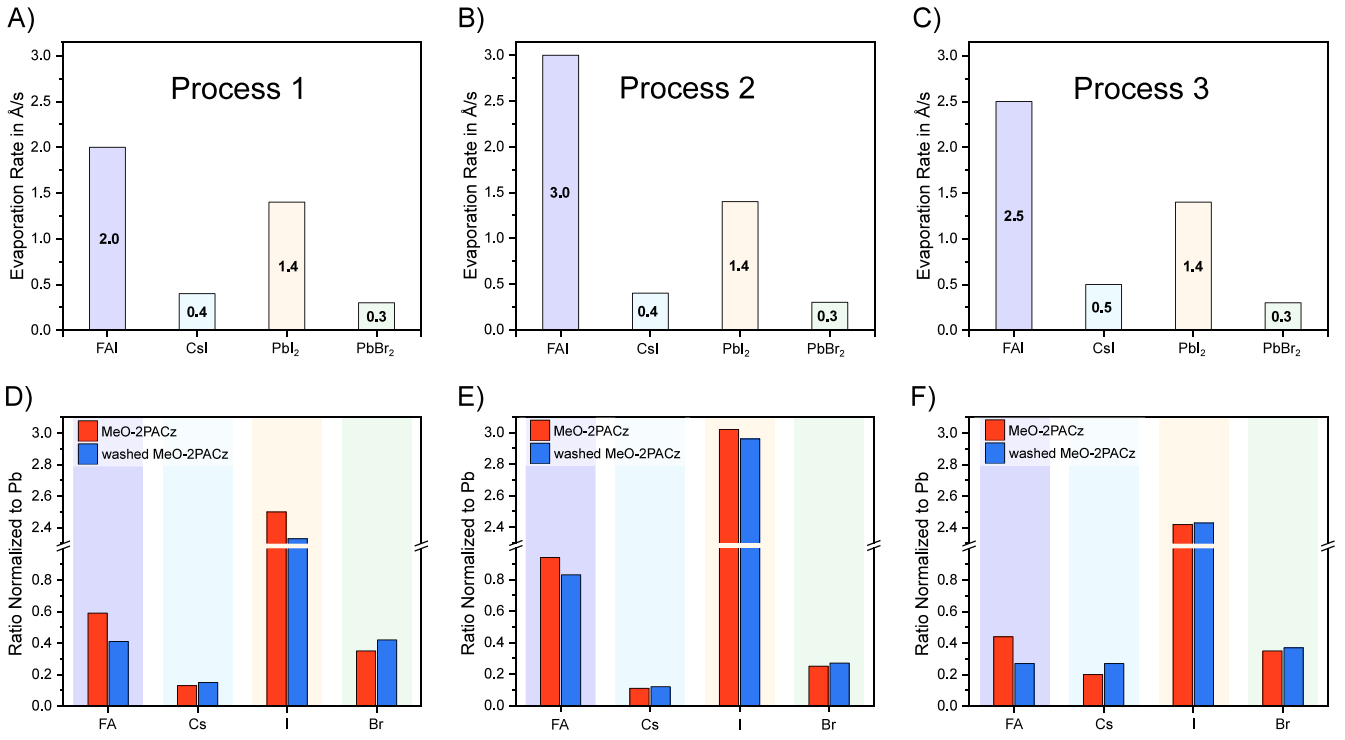

Figure 5. (A–C) Evaporation rates of three different coevaporation processes. (D,E) Composition of the resulting perovskite films normalized to lead. For all processes a comparison of perovskite composition measured by ^{1}H NMR and T-XRF on pristine MeO-2PACz (red) and washed MeO-2PACz (blue) is shown. The solar cell performance for process 1 is shown in Figure 1 while the data for processes 2 and 3 are displayed in Figures S6 and S7.

film, analyzed with the new method presented here. Morphologically, there are pronounced differences among the films. On washed MeO2-PACz small and porous grains are formed, while large columnar grains are visible for pristine MeO-2PACz. Furthermore, the perovskite layer grown on washed MeO-2PACz is about 10% thinner in comparison to pristine MeO-2PACz. The overall mass (sum of each component in Figure 3) of perovskite is 1.296 mg for washed MeO-2PACz and 1.423 mg for pristine MeO-2PACz. This difference fits well with the observed variation in the layer thickness.

The absolute amount of Pb is comparable between that of MeO-2PACz and that of washed MeO-2PACz. A strong difference is present for FA^+ and I. This shows that during coevaporation on washed MeO-2PACz, not only less FAI is incorporated into the perovskite lattice (as implied by changes in EQE and XRD), but the total amount of FAI that is present on the substrate is significantly lower. Interestingly, slightly higher Cs and Br contents can be seen on washed MeO-2PACz. Presumably, the lack of FAI favors the incorporation of Cs and Br to fill the anion and cation vacancies. As the amount of Pb is almost the same on pristine and washed MeO-2PACz and as precursors PbI_2, $PbBr_2$, CsI, and FAI are used, some halide exchange reactions need to happen during the coevaporation process.

To understand how variations in the evaporation rate influence the perovskite composition, perovskite films from two additional processes (Processes 2 and 3) were analyzed and compared to a reference process (Process 1). The data presented above (Figures 3 and 4) originate from films prepared via the reference Process 1. Process 2 features only a higher FAI rate as compared to the reference Process 1, while in Process 3 both FAI and CsI rates were increased. Figure 5A–C highlights all evaporation rates of the three processes as a bar chart. In Figure 5D–F the composition of the films, as determined from NMR and T-XRF, is displayed for perovskites on pristine (red) and washed (blue) MeO-2PACz. A comparison between Process 1 (Figure 5A,D) and Process 2 (Figure 5B,E) shows that the 50% increase in FAI rate directly results in an increase in the I^- and FA^+ content of the film. Furthermore, it is striking that the increased incorporation of FAI for pristine MeO-2PACz, observed in Process 1, is also valid for Process 2, even though a 50% higher FAI rate was used and one might expect a saturation of the FAI incorporation. In solar cells (Figure S6A) the higher FAI rate of Process 2 leads to an increased efficiency on washed MeO-2PACz. However, for pristine MeO-2PACz the high FAI rate causes a considerable drop in efficiency to ~6% (Figure S6A). This indicates an excess of FAI, which is consistent with the absence of PbI_2 in the XRD pattern (Figure S6C). Both the Cs and Br contents decreased slightly in Process 2, although the same evaporation rates of $PbBr_2$ and CsI as in Process 1 were used. This indicates that due to the higher evaporation rate of FAI, cesium and bromide are partially replaced by FA^+ and iodide. When comparing Process 1 (Figure 5A,D) to Process 3 (Figure 5C,F) the most striking feature is that, although the FAI rate was increased by 25%, less FA^+ can be found in the films compared to Process 1. Apparently, the small increase from 0.4 to 0.5 Å/s in the CsI rate strongly influences the incorporation of FA^+. This indicates a change in the reaction kinetics and shows that Cs and FA^+ are competing to occupy the A-side position in the perovskite. The slightly higher Cs content leads to a higher band gap in comparison to Process 1, visible in the EQE (Figure S7D). The solar cells of

https://doi.org/10.1021/acsenergylett.5c03689
ACS Energy Lett. 2026, 11, 1935−1943

Process 3 reach a higher PCE on pristine MeO-2PACz (~18%) than on washed MeO-2PACz (~13%) (Figure S7A).

Overall, the increased incorporation of FA^+ on pristine MeO-2PACz is observed for all processes, even for Process 2, where the very high FAI rate leads to an excess of organic precursors in the films. The comparison of the three different processes shows that changes in the evaporation rates influence the composition of the resulting films to a great extent. However, changes in the evaporation rates are not always transferred linearly into corresponding changes in perovskite stoichiometry, which complicates the optimization of coevaporation processes and makes the composition control based on evaporation rates measured by QCMs challenging. Our new method, which allows to determine the exact composition of the perovskite material, can help to improve the understanding of the coevaporation process and to further optimize the vacuum-based deposition of perovskite solar cells.

In this work, we developed a straightforward and efficient method to analyze the absolute composition of hybrid metal halide perovskites. With a combination of nuclear magnetic resonance spectroscopy (NMR) and total reflection X-ray fluorescence spectroscopy (T-XRF) we can quantify all elements of the perovskite material. Using a mixture of two internal standards allows us to simplify the sampling process, as the perovskite film can be directly dissolved, and no scratching and scaling of perovskite powder is necessary. Initially, the accuracy and repeatability of the method are evaluated using different precursor powder samples. For all tested samples, the deviations (relative standard deviation and relative median absolute deviation) remain below 10% irrespective of sample complexity, from binary systems such as FAI + MABr to triple-cation mixtures. Subsequently, we use the developed method to investigate the coevaporation process of formamidinium-cesium mixed-halide perovskites. We show that the preparation process of the underlying hole transport material MeO-2PACz has a strong effect on the resulting perovskite composition: for all tested process conditions, perovskite films prepared on washed MeO-2PACz contain a smaller amount of FAI than films on pristine MeO-2PACz. The differences in FAI incorporation directly influence the Br/I ratio and, therefore, the band gap of perovskite films. All in all, the film compositions determined by ^{1}H NMR and T-XRF show a good agreement with the perovskite stoichiometry inferred from XRD and EQE measurements. A comparison of different coevaporation processes shows that the evaporation rates do not always have a linear impact on the composition of the film. For example, a small increase in the CsI rate strongly reduces the level of incorporation of FA^+, indicating that Cs^+ and FA^+ are competing to occupy the A-side position in the perovskite. Our results highlight the importance of compositional analysis to gain insight into the complex coevaporation process and underscores its crucial role in achieving high-performance perovskite solar cells.

■ ASSOCIATED CONTENT

Supporting Information

The Supporting Information is available free of charge at https://pubs.acs.org/doi/10.1021/acsenergylett.5c03689.

Figures S1−S9 and experimental section (materials, perovskite film and solar cell preparation, details on composition analysis, and solar cell characterization) (PDF)

■ AUTHOR INFORMATION

Corresponding Author

Marcel Roß − *Department Perovskite Tandem Solar Cells, Helmholtz-Zentrum Berlin (HZB), 12489 Berlin, Germany;* orcid.org/0000-0002-5916-8540; Email: marcel.ross@helmholtz-berlin.de

Authors

Stefanie Severin − *Department Perovskite Tandem Solar Cells, Helmholtz-Zentrum Berlin (HZB), 12489 Berlin, Germany*

Jana Hildebrandt − *Humboldt-Universität zu Berlin, 12489 Berlin, Germany*

Kerstin Erdmann − *Bundesanstalt für Materialforschung und -Prüfung (BAM), 12489 Berlin, Germany*

Aleksandra Miaskiewicz − *Department Perovskite Tandem Solar Cells, Helmholtz-Zentrum Berlin (HZB), 12489 Berlin, Germany*

Viktor Škorjanc − *Department Perovskite Tandem Solar Cells, Helmholtz-Zentrum Berlin (HZB), 12489 Berlin, Germany*

Wander Max Bernardes de Araujo − *Department Perovskite Tandem Solar Cells, Helmholtz-Zentrum Berlin (HZB), 12489 Berlin, Germany*

Matthew Leyden − *Department Perovskite Tandem Solar Cells, Helmholtz-Zentrum Berlin (HZB), 12489 Berlin, Germany*

Lars Korte − *Department Perovskite Tandem Solar Cells, Helmholtz-Zentrum Berlin (HZB), 12489 Berlin, Germany;* orcid.org/0000-0002-9207-9048

Stefan Seeger − *Bundesanstalt für Materialforschung und -Prüfung (BAM), 12489 Berlin, Germany*

André Dallmann − *Humboldt-Universität zu Berlin, 12489 Berlin, Germany*

Steve Albrecht − *Department Perovskite Tandem Solar Cells, Helmholtz-Zentrum Berlin (HZB), 12489 Berlin, Germany; Faculty of Electrical Engineering and Computer Science, Technical University Berlin, 10587 Berlin, Germany;* orcid.org/0000-0001-9962-9535

Complete contact information is available at: https://pubs.acs.org/10.1021/acsenergylett.5c03689

Notes

The authors declare no competing financial interest.
The author Stefan Seeger is retired from BAM.

■ ACKNOWLEDGMENTS

The authors acknowledge the Helmholtz Association for funding within the HySPRINT Innovation lab and the Zeitenwende project as well as the Federal Ministry of Education and Research (BMWK) for funding the project SHAPE (grant no. 03EE1123C). The authors received funding from the German State of Lower Saxony in project "NextGenPV", through funding program "zukunft.niedersachsen". The Energy Materials In-situ Laboratory Berlin (EMIL) operated by the Helmholtz-Zentrum für Materialien und Energie GmbH (HZB) is acknowledged for granting access to its sample characterization laboratory. The authors thank T. Lußky, J. Beckedahl, H. Heinz, C. Ferber and M. Choyne for technical assistance.

REFERENCES

(1) Correa-Baena, J.-P.; Abate, A.; Saliba, M.; Tress, W.; Jesper Jacobsson, T.; Grätzel, M.; Hagfeldt, A. The rapid evolution of highly efficient perovskite solar cells. *Energy Environ. Sci.* **2017**, *10* (3), 710.

(2) Gil-Escrig, L.; Roß, M.; Sutter, J.; Al-Ashouri, A.; Becker, C.; Albrecht, S. Fully vacuum-processed perovskite solar cells on pyramidal microtextures. *Sol RRL* **2021**, *5* (1), 2000553.

(3) Cojocaru, L.; Wienands, K.; Kim, T. W.; Uchida, S.; Bett, A. J.; Rafizadeh, S.; Goldschmidt, J. C.; Glunz, S. W. Detailed investigation of evaporated perovskite absorbers with high crystal quality on different substrates. *ACS Appl. Mater. Interfaces* **2018**, *10* (31), 26293.

(4) Li, J.; Dewi, H. A.; Wang, H.; Zhao, J.; Tiwari, N.; Yantara, N.; Malinauskas, T.; Getautis, V.; Savenije, T. J.; Mathews, N.; et al. Co-Evaporated MAPbI3 with Graded Fermi Levels Enables Highly Performing, Scalable, and Flexible p-i-n Perovskite Solar Cells. *Adv. Funct. Mater.* **2021**, *31*, 2103252.

(5) Roß, M.; Severin, S.; Stutz, M. B.; Wagner, P.; Köbler, H.; Favin-Lévêque, M.; Al-Ashouri, A.; Korb, P.; Tockhorn, P.; Abate, A.; et al. Co-evaporated formamidinium lead iodide based perovskites with 1000 h constant stability for fully textured monolithic perovskite/silicon tandem solar cells. *Adv. Energy Mater.* **2021**, *11*, 2101460.

(6) Chiang, Y.-H.; Frohna, K.; Salway, H.; Abfalterer, A.; Pan, L.; Roose, B.; Anaya, M.; Stranks, S. D. Vacuum-deposited wide-bandgap perovskite for all-perovskite tandem solar cells. *ACS Energy Letters* **2023**, *8* (6), 2728.

(7) Gil-Escrig, L.; Dreessen, C.; Palazon, F.; Hawash, Z.; Moons, E.; Albrecht, S.; Sessolo, M.; Bolink, H. J. Efficient wide-bandgap mixed-cation and mixed-halide perovskite solar cells by vacuum deposition. *ACS Energy Lett.* **2021**, *6* (2), 827.

(8) Škorjanc, V.; Miaskiewicz, A.; Roß, M.; Maniyarasu, S.; Severin, S.; Leyden, M. R.; Holzhey, P.; Ruske, F.; Korte, L.; Albrecht, S. Seed layers for wide-band gap coevaporated perovskite solar cells: Cscl regulates band gap and reduces process variability. *ACS Energy Letters* **2024**, *9* (11), 5639.

(9) Wolter, S. J.; Steckenreiter, V.; Tatarzyn, M. C.; Wietler, T.; Niepelt, R.; Kajari-Schroder, S. Determination and influence evaluation of the acoustic impedance ratio for thermal co-evaporation. *Appl. Phys. Lett.* **2018**, *113* (1), 4.

(10) Lohmann, K. B.; Patel, J. B.; Rothmann, M. U.; Xia, C. Q.; Oliver, R. D. J.; Herz, L. M.; Snaith, H. J.; Johnston, M. B. Control over crystal size in vapor deposited metal-halide perovskite films. *ACS Energy Lett.* **2020**, *5* (3), 710.

(11) Roß, M.; Gil-Escrig, L.; Al-Ashouri, A.; Tockhorn, P.; Jošt, M.; Rech, B.; Albrecht, S. Co-Evaporated p-i-n Perovskite Solar Cells beyond 20% Efficiency: Impact of Substrate Temperature and Hole-Transport Layer. *ACS Appl. Mater. Interfaces* **2020**, *12* (35), 39261.

(12) Abzieher, T.; Feeney, T.; Schackmar, F.; Donie, Y. J.; Hossain, I. M.; Schwenzer, J. A.; Hellmann, T.; Mayer, T.; Powalla, M.; Paetzold, U. W. From groundwork to efficient solar cells: On the importance of the substrate material in co-evaporated perovskite solar cells. *Adv. Funct. Mater.* **2021**, *31* (42), 2104482.

(13) Olthof, S.; Meerholz, K. Substrate-dependent electronic structure and film formation of MAPbI3 perovskites. *Sci. Rep* **2017**, *7* (1), 40267.

(14) Borchert, J.; Leychuk, I.; Snoek, L. C.; Rothmann, M. U.; Haver, R.; Snaith, H. J.; Brabec, C. J.; Herz, L. M.; Johnston, M. B. Impurity tracking enables enhanced control and reproducibility of hybrid perovskite vapor deposition. *ACS Appl. Mater. Interfaces* **2019**, *11* (32), 28851.

(15) Kroll, M.; Öz, S. D.; Zhang, Z.; Ji, R.; Schramm, T.; Antrack, T.; Vaynzof, Y.; Olthof, S.; Leo, K. Insights into the evaporation behaviour of fai: material degradation and consequences for perovskite solar cells. *Sustainable Energy & Fuels* **2022**, *6* (13), 3230.

(16) Roß, M.; Stutz, M. B.; Albrecht, S. Revealing the role of methylammonium iodide purity on the vapor-phase deposition process of perovskites. *Solar RRL* **2022**, *6* (10), 2200500.

(17) Pareja-Rivera, C.; Solís-Cambero, A. L.; Sánchez-Torres, M.; Lima, E.; Solis-Ibarra, D. On the true composition of mixed-cation perovskite films. *ACS Energy Letters* **2018**, *3* (10), 2366.

(18) Eliseev, E. A.; Filatova, D. G.; Chizhov, A. S.; Rumyantseva, M. N.; Gaskov, A. M. Simple in situ analysis of metal halide perovskite-based sensor materials using micro x-ray fluorescence and inductively coupled plasma mass spectrometry. *Mendeleev Commun.* **2021**, *31* (4), 462.

(19) Heinze, K. L.; Schulz, T.; Scheer, R.; Pistor, P. Structural evolution of sequentially evaporated (cs,fa)pb(i,br)3 perovskite thin films via in situ x-ray diffraction. *physica status solidi (a)* **2024**, *221* (3), 2300690.

(20) Teuscher, J.; Ulianov, A.; Müntener, O.; Grätzel, M.; Tétreault, N. Control and study of the stoichiometry in evaporated perovskite solar cells. *ChemSusChem* **2015**, *8* (22), 3847.

(21) Abzieher, T.; Muzzillo, C. P.; Mirzokarimov, M.; Lahti, G.; Kau, W. F.; Kroupa, D. M.; Cira, S. G.; Hillhouse, H. W.; Kirmani, A. R.; Schall, J.; et al. Continuous flash sublimation of inorganic halide perovskites: overcoming rate and continuity limitations of vapor deposition. *Journal of Materials Chemistry A* **2024**, *12* (14), 8405.

(22) Heslop-Harrison, J. S. Energy Dispersive X-Ray Analysis. In *Physical Methods in Plant Sciences*; Springer Berlin Heidelberg: 1990; pp 244–277. DOI: 10.1007/978-3-642-83611-4_9.

(23) Hodoroaba, V.-D.; Rackwitz, V. Gaining improved chemical composition by exploitation of compton-to-rayleigh intensity ratio in xrf analysis. *Anal. Chem.* **2014**, *86* (14), 6858.

(24) Al-Hakkani, M. F. Guideline of inductively coupled plasma mass spectrometry "icp-ms": fundamentals, practices, determination of the limits, quality control, and method validation parameters. *SN Applied Sciences* **2019**, *1* (7), 791.

(25) Flores, E. M.; Mello, P. A.; Krzyzaniak, S. R.; Cauduro, V. H.; Picoloto, R. S. Challenges and trends for halogen determination by inductively coupled plasma mass spectrometry: A review. *Rapid Commun. Mass Spectrom.* **2020**, *34* (S3), e8727.

(26) Villemant, B.; Noël, J.; Caron, B. Cl, br and i measurements in rock samples by icp-ms/ms using reaction gases. *Chem. Geol.* **2025**, *681*, 122681.

(27) Hojo, M.; Yamamoto, M.; Okamura, K. Dilute nitric or nitrous acid solution containing halide ions as effective media for pure gold dissolution. *Phys. Chem. Chem. Phys.* **2015**, *17* (30), 19948.

(28) Linge, K. L.; Jarvis, K. E. Quadrupole icp-ms: Introduction to instrumentation, measurement techniques and analytical capabilities. *Geostandards and Geoanalytical Research* **2009**, *33* (4), 445.

(29) Louie, H.; Wong, C.; Huang, Y. J.; Fredrickson, S. A study of techniques for the preservation of mercury and other trace elements in water for analysis by inductively coupled plasma mass spectrometry (icp-ms). *Anal. Methods* **2012**, *4* (2), 522.

(30) Wobrauschek, P. Total reflection x-ray fluorescence analysis. *X-Ray Spectrometry* **2007**, *36* (5), 289.

(31) Berneike, W.; Knoth, J.; Schwenke, H.; Weisbrod, U. Surface analysis for si-wafers using total reflection x-ray fluorescence analysis. *Z. Anal. Chem.* **1989**, *333* (4–5), 524.

(32) Seeger, S.; Osan, J.; Czömpöly, O.; Gross, A.; Stosnach, H.; Stabile, L.; Ochsenkuehn-Petropoulou, M.; Tsakanika, L. A.; Lymperopoulou, T.; Goddard, S.; et al. Quantification of element mass concentrations in ambient aerosols by combination of cascade impactor sampling and mobile total reflection x-ray fluorescence spectroscopy. *Atmosphere* **2021**, *12* (3), 309.

(33) Dally, P.; Messou, D.; Robillard, M.; Cacovich, S.; Yaiche, A.; Rousset, J.; Etcheberry, A.; Bouttemy, M. Probing the chemistry of perovskite systems by xps and gd-oes depth-profiling: Potentials and limitations, *2021 IEEE 48th Photovoltaic Specialists Conference (PVSC)*; IEEE: 2021; pp 0931–0934. DOI: 10.1109/pvsc43889.2021.9518696.

(34) Hu, J.; Wang, D.; Shi, Y.; Ahmad, N.; Sun, M.; Wang, Y.; Yang, H.; Zhang, D.; Hu, Q.; Luo, D.; et al. Best practice of identifying chemical constituents and evolution of sn-containing perovskites by photoelectron spectroscopy. *J. Phys. Chem. Lett.* **2025**, *16* (43), 11167.

(35) Ralaiarisoa, M.; Frisch, J.; Frégnaux, M.; Cacovich, S.; Yaïche, A.; Rousset, J.; Gorgoi, M.; Ceratti, D. R.; Kodalle, T.; Roncoroni, F. Influence of x-ray irradiation during photoemission studies on halide perovskite-based devices. *Small Methods* **2023**, *7* (11), 2300458.

(36) Lin, W.-C.; Lo, W.-C.; Li, J.-X.; Wang, Y.-K.; Tang, J.-F.; Fong, Z.-Y. In situ xps investigation of the x-ray-triggered decomposition of perovskites in ultrahigh vacuum condition. *npj Materials Degradation* **2021**, *5* (1), 13.
(37) Philippe, B.; Park, B.-W.; Lindblad, R.; Oscarsson, J.; Ahmadi, S.; Johansson, E. M. J.; Rensmo, H. Chemical and electronic structure characterization of lead halide perovskites and stability behavior under different exposures—a photoelectron spectroscopy investigation. *Chem. Mater.* **2015**, *27* (5), 1720.
(38) Al-Ashouri, A.; Magomedov, A.; Roß, M.; Jost, M.; Talaikis, M.; Chistiakova, G.; Bertram, T.; Marquez, J. A.; Kohnen, E.; Kasparavicius, E.; et al. Conformal monolayer contacts with lossless interfaces for perovskite single junction and monolithic tandem solar cells. *Energy Environ. Sci.* **2019**, *12* (11), 3356.
(39) Kerner, R. A.; Christensen, E. D.; Harvey, S. P.; Messinger, J.; Habisreutinger, S. N.; Zhang, F.; Eperon, G. E.; Schelhas, L. T.; Zhu, K.; Berry, J. J.; et al. Analytical evaluation of lead iodide precursor impurities affecting halide perovskite device performance. *ACS Applied Energy Materials* **2023**, *6* (1), 295.
(40) Feeney, T.; Petry, J.; Torche, A.; Hauschild, D.; Hacene, B.; Wansorra, C.; Diercks, A.; Ernst, M.; Weinhardt, L.; Heske, C.; et al. Understanding and exploiting interfacial interactions between phosphonic acid functional groups and co-evaporated perovskites. *Matter* **2024**, *7* (6), 2066.
(41) Yan, S.; Patel, J. B.; Lee, J. E.; Elmestekawy, K. A.; Ratnasingham, S. R.; Yuan, Q.; Herz, L. M.; Noel, N. K.; Johnston, M. B. A templating approach to controlling the growth of coevaporated halide perovskites. *ACS Energy Letters* **2023**, *8* (10), 4008.
(42) Leyden, M. R.; Škorjanc, V.; Miaskiewicz, A.; Severin, S.; Maniyarasu, S.; Gries, T.; Beckedahl, J.; Scheler, F.; Simmonds, M.; Holzhey, P. Loading precursors into self-assembling contacts for improved performance and process control in evaporated perovskite solar cells. *Solar RRL* **2024**, *8* (21), 2400575.
(43) Öz, S. D.; Olthof, S. Effect of hole extraction layer on the composition of thermally evaporated formamidinium-based mixed halide perovskites. *ACS Appl. Mater. Interfaces* **2025**, *17* (16), 24535.

https://doi.org/10.1021/acsenergylett.5c03689
ACS Energy Lett. 2026, 11, 1935−1943